CONSTITUTIVE RELATIONSHIPS FOR ALIGNED DISCONTINUOUS FIBER COMPOSITES

R. Byron Pipes
Douglas W. Coffin

Department of Mechanical Engineering
Center for Composite Materials
University of Delaware
Newark, Delaware 19716

ABSTRACT

Predictions for the effective viscosities of a hyper-anisotropic medium consisting of collimated, discontinuous fibers suspended in a viscous matrix developed earlier by the authors [1-3] have been extended to capture the characteristics of typical polymers including non-Newtonian behavior and temperature dependence. In addition, the influence of fiber misorientation has also been modeled by compliance averaging to determine ensemble properties for a given orientation distribution.

1. Anisotropic Viscosities of an Oriented Fiber Assembly with Temperature and Strain Rate Dependence

Introduction

In several earlier papers [1-3] the authors developed models which predict the primary viscosities of an anisotropic incompressible material consisting of collimated, long discontinuous fibers suspended in a fluid matrix. A state of transverse isotropic symmetry was assumed for the medium. These models were developed by assuming the kinematics of adjacent rigid fibers and determining the resulting behavior of the matrix fluid. This procedure allows for the prediction of the effective properties of the medium including longitudinal elongational, in-plane shearing, transverse elongational and transverse shearing viscosities. Explicit expressions have been developed for each of the effective viscosities for a Newtonian matrix fluid. Table 1 shows a summary of these results in terms of fiber volume fraction, f, fiber aspect ratio, L/D, and matrix viscosity, η.

A deficiency of the simple power-law constitutive relation for a shear thinning fluid is its lack of a finite zero-shear viscosity. In a recent paper [4] the authors introduced a constitutive relation which exhibits a finite zero-shear rate viscosity and includes a temperature dependence into the relations for the effective material properties. This development will be summarized in the following.

1.1 Development

The effective viscosities shown in Table 1 fail to capture all the characteristics exhibited by polymer melts such as dependence on shear rate and temperature. Carreau [5,6] has introduced the following empirical rheological model to describe the non-Newtonian behavior of such a fluid.

$$\eta = \bar{\eta}_0 \left[1 + (\bar{\lambda}\dot{\gamma})^2\right]^{(n-1)/2} \qquad (1)$$

The onset of the nonlinearity is determined by the time constant, $\bar{\lambda}$. It is clear from equation (1) that for $(\bar{\lambda}\ \dot{\gamma})<<1$ the viscosity becomes Newtonian. The power law exponent, n, determines the degree of nonlinearity. The value of n=1 corresponds to a Newtonian fluid, and as the exponent decreases the fluid exhibits increased shear thinning.

It has been stated [7] that the influence of temperature on viscosity can be represented as follows:

$$\bar{\eta}_0 = \eta_0 A_T\ ;\ \bar{\lambda} = \lambda A_T \tag{2}$$

where the temperature shift factor, A_T, is defined as:

$$A_T = e^{-\xi(T/T_0-1)} \tag{2a}$$

Note, the temperature shift factor as defined above is normalized so that at a given reference temperature, T_0, the shift factor equals unity.

Viscosity versus shear rate data for typical high performance polymer PEEK at 399°C [8] is shown in Figure 1. Figure 2 shows the temperature shift factor versus temperature for PEEK [8]. Equation (1) and equation (2a) were fit to the PEEK data thus determining the parameters as follows:

$$\eta_0 = 280 \text{ Pa-S},\ \lambda = 0.038 \text{ S},\ n = 0.787,\ \xi = 6.56$$

Equations (1) and (2a) are compared with the experimental data in Figures 1 and 2.

Employing this matrix constitutive relation and the development presented in reference [3] it is possible to derive new expressions for effective viscosities of the medium as follows:

$$\eta_{11} = \frac{\eta_0 A_T (1-\mu) f}{2\mu} (L/D)^2 \left[1 + \frac{A_T^2 (1-\mu)^2 (L/D)^2}{4\mu^2} (\lambda \dot{\varepsilon}_1)^2 \right]^{(n-1)/2} \tag{3a}$$

$$\eta_{12} = \frac{\eta_0 A_T(1+\mu)}{2\mu}\left[1+\frac{A_T^2(1+\mu)^2}{4\mu^2}(\lambda\dot{\gamma}_{12})^2\right]^{(n-1)/2} \tag{3c}$$

$$\eta_{23} = \frac{\eta_0 A_T}{\mu}\left[1+\frac{A_T^2}{\mu^2}(\lambda\dot{\gamma}_{23})^2\right]^{(n-1)/2} \tag{3d}$$

where

$$\mu = 1-\sqrt{f/F}\ ;\ F = \begin{cases} \dfrac{\pi}{4} & \text{square array} \\ \dfrac{\pi}{2\sqrt{3}} & \text{hexagonal array} \end{cases} \tag{3e}$$

1.2 Results

Given the material descriptors and matrix properties as a function of temperature and strain rate, equations (3a-d) can be utilized to predict the unique properties of the material. Figure 3 shows these predictions for the PEEK data discussed in section 2 in conjunction with a square array of 60 percent fiber volume content and a fiber aspect ratio of 10^4. The figure illustrates the relative difference in the various effective viscosities. It is especially interesting that the maximum Newtonian strain rate is lower for the fiber filled polymer than for the neat polymer. This is especially evident in the longitudinal elongational viscosity which begins to exhibit the shear thinning phenomenon at an elongational strain rate approximately three magnitudes of order less than the fluid's maximum Newtonian strain rate.

Figure 4 shows the effect of temperature on the in-plane viscosity versus strain rate. Notice that an increase in temperature decreases the viscosity but increases the maximum range in rate over which Newtonian behavior is observed.

To gain a better understanding of the strain rate and temperature dependence a parametric study of the Carreau model parameters will be presented. Only the longitudinal elongational viscosity will be illustrated since the same general tendencies will hold for all the viscosities in equation (3). For

large strain rate, it is clear that the quantity (n-1) defines the slope of the viscosity versus strain rate curve on a log-log scale. This is illustrated in Figure 5 for values of the power law term in the range 0-1. Note that n=1 corresponds to the Newtonian case. Using a log-log bi-linear approximation for the viscosity strain rate relation, an upper bound for the maximum Newtonian strain rate is

$$\dot{\varepsilon}_N = \frac{2\mu}{A_T(1-\mu)(L/D)\lambda} \tag{4}$$

Equation (4) shows that as the time constant increases, $\dot{\varepsilon}_N$ decreases. This effect of the time constant on $\dot{\varepsilon}_N$ is illustrated in Figure 6. The influence of the fiber geometry on viscosity can also be observed by studying equation (4). Increases in L/D will result in a decrease in the maximum Newtonian Strain rate for the fiber assembly. The temperature dependency on the viscosity appears in the zero-shear viscosity and time constant. As the temperature shift factor increases, the zero-shear viscosity and the time constant decrease. This is illustrated in Figure 7 for various values of the temperature shift factor.

2. Influence of Fiber Orientation on the Viscosities of Anisotropic Materials

The relationships for the material properties as presented above are valid for a system of perfectly aligned fibers which coincides with the reference axes. Many times the fibers are off axis to the loads and hence the reference axis. In this case the effective properties are of interest. Also due to manufacturing and processing, the fibers are not perfectly aligned. The effective viscosities for these two conditions will be studied in the following.

The effective viscosities for a medium consisting of collimated, long discontinuous fibers suspended in a viscous matrix were examined in the last section. These results have shown that the effective viscosities for such a system are highly anisotropic with anisotropy ratios which often exceed 10^6 for fiber aspect ratios of 10^3 - 10^4. Given the extreme sensitivity to material anisotropy of material properties transformed outside the principal material coordinate system, it is clear that

fiber orientation will have a great influence upon effective material properties. Two conditions of fiber orientation must be considered. First, the condition where fibers are perfectly collimated but do not coincide with the load direction and second, the condition where individual fibers are misoriented with respect to the principal material direction. In the latter case, misorientation of individual fibers might have occurred during the manufacturing step, while in the former case the inability to insure that the test directions and material principal directions coincide could lead to measurement of properties which could differ greatly from actual values.

2.1 Transformed Properties

For orthotropic viscous materials in plane stress with the principal material designated "1", the principal viscosities are:

η_{11} : longitudinal elongational viscosity

η_{22} : transverse elongational viscosity

η_{12} : inplane shearing viscosity

The apparent or transformed properties at any angle, θ may be expressed in terms of the principal viscosities and the angle, θ.

$$\eta_{11}'(\theta)/\eta_{11} = \left[m^4 + (\eta_{11}/\eta_{12}-1)m^2n^2 + (\eta_{11}/\eta_{22})n^4\right]^{-1} \quad (5)$$

$$\eta_{22}'(\theta)/\eta_{22} = \left[m^4 + (\eta_{22}/\eta_{12}-\eta_{22}/\eta_{11})m^2n^2 + (\eta_{22}/\eta_{11})n^4\right]^{-1} \quad (6)$$

$$\eta_{12}'(\theta)/\eta_{12} = \left[(m^2-n^2)^2 + 4(2\eta_{12}/\eta_{11}+\eta_{12}/\eta_{22})m^2n^2\right]^{-1} \quad (7)$$

where $m = \cos\theta$ and $n = \sin\theta$.

Results for η_{11}', η_{22}', and η_{12}' are shown in Figures 8-10 where estimates for η_{11}, η_{22}, and η_{12} are taken from reference [1] as shown in Table 2. Estimates for the viscosities could also be obtained from the relations given in equations 3a-3c. The dependence of the principal elongational viscosity upon fiber aspect ratio (L/D) is apparent in Figure 8. For systems with $L/D=10^4$ the ratio

of transformed elongational viscosity to principal elongational viscosity, η'_{11}/η_{11} is 10^{-2} at $\theta=1°$. Hence, fiber aspect ratios which correspond to actual material systems such as that discussed in reference [9] yield highly anisotropic materials systems whose properties exhibit extreme sensitivity to fiber orientation. A similar result for η'_{22}/η_{22} is shown in Figure 9 for $L/D=10^4$. For the apparent inplane shearing viscosity η'_{12}/η_{12}, the maximum occurs at $\theta=\pi/4$ with a value of approximately 10^1 as shown in Figure 10. It is interesting to note that while both the elongational viscosities varied over 10^0 to 10^{-6} for the range in orientation angle of 0 to $\pi/2$, the inplane shearing viscosity ratio only varied over 10^0 to 10^1 for $L/D=10^4$.

2.2 Ensemble Properties

Should the material system consist of an ensemble of elements (fibers) with varying orientation, the expected value of the viscosities for the ensemble will be different from the values obtained from equations 5-7. In fact, even with small misalignments the effective viscosities may be drastically different. The effective viscosities will be bounded by average values as determined by assuming constant stress or constant strain. In the following, only the expected values based on constant stress will be presented. This will illustrate the large changes in effective viscosity due to small misorientations.

To determine the expected values of the viscosities, a distribution function, $\phi(\theta)$, representing the fiber orientation is determined and a weighted average of the compliance matrix is calculated as shown below.

$$\langle \eta_{ij} \rangle_\beta = \left[\int_{-\pi/2}^{\pi/2} \beta'_{ij}(\theta)\phi(\theta)d\theta \right]^{-1} \tag{8}$$

where the compliance terms, $\beta'_{ij}(\theta)$, are defined as follows:

$$\beta'_{11} = m^4/\eta_{11} + (-1/\eta_{11}+1/\eta_{12})\, m^2n^2 + n^4/\eta_{22} \tag{9}$$

$$\beta'_{22} = n^4/\eta_{11} + (-1/\eta_{11}+1/\eta_{12})\, m^2n^2 + m^4/\eta_{22} \tag{10}$$

$$\beta'_{66} = m^4/\eta_{12} + (8/\eta_{11} + 4/\eta_{22} - 2/\eta_{12})\, m^2 n^2 + n^4/\eta_{12} \tag{11}$$

If the fibers are assumed to be uniformly distributed between $\pm\theta_1$, the normalized probability density function is

$$\begin{aligned} &\phi = 0,\ \theta > \theta_1 \text{ and } \theta < -\theta_1 \\ &\phi = 1/2\theta_1,\ -\theta_1 \le \theta \le \theta_1 \end{aligned} \tag{12}$$

Combining equations (8) through (12) yields the expected value of the viscosities utilizing the compliance matrix:

$$\begin{aligned} \langle\eta_{11}\rangle/\eta_{11} = {} & 32\theta_1\eta_{22}\eta_{12}/[(2\eta_{22}\eta_{12} + 3\eta_{11}\eta_{12} + \eta_{11}\eta_{22})\, 4\theta_1 \\ & + (\eta_{12}\eta_{22} - \eta_{11}\eta_{12})\, 8\sin 2\theta_1 + (2\eta_{22}\eta_{12} + \eta_{11}\eta_{12} - \eta_{11}\eta_{22})\, \sin 4\theta_1] \end{aligned} \tag{13}$$

$$\begin{aligned} \langle\eta_{22}\rangle/\eta_{22} = {} & 32\theta_1\eta_{11}\eta_{12}/[(2\eta_{22}\eta_{12} + 3\eta_{11}\eta_{12} + \eta_{11}\eta_{22})\, 4\theta_1 \\ & + (\eta_{11}\eta_{12} - \eta_{22}\eta_{12})\, 8\sin 2\theta_1 + (2\eta_{22}\eta_{12} + \eta_{11}\eta_{12} - \eta_{11}\eta_{22})\, \sin 4\theta_1] \end{aligned} \tag{14}$$

$$\begin{aligned} \langle\eta_{12}\rangle/\eta_{12} = {} & 8\theta_1\eta_{11}\eta_{22}/[(\eta_{11}\eta_{22} + 2\eta_{12}\eta_{22} + \eta_{11}\eta_{12})\, 4\theta_1 \\ & + (\eta_{11}\eta_{22} - 2\eta_{12}\eta_{22} - \eta_{11}\eta_{12})\, \sin 4\theta_1] \end{aligned} \tag{15}$$

Consider the expected value of the principal elongational viscosity $\langle\eta_{11}\rangle$ for a fiber ensemble with equal probability of fiber orientation between $\pm\theta_1$. The expected viscosity for a range of values of θ_1 are shown in Figure 11. These results indicate that the compliance method mirrors the significant sensitivity to orientation shown for η'_{11} in Figure 8. Therefore for small misalignment of the fibers the apparent viscosity is greatly reduced.

For the expected value of the transverse elongational viscosity $\langle\eta_{11}\rangle$ of the ensemble, there is little dependence on the misorientation as shown in Figure 12. Similar results for the expected value of the shearing viscosity $\langle\eta_{11}\rangle$ are shown in Figure 13.

3.0 Conclusions

Relations for predicting the effective viscosities of an aligned discontinuous fiber filled fluid developed in [1-3] for Newtonian and power law fluids have been extended to include zero-shear viscosity and temperature dependence. This was accomplished by describing the matrix fluid viscosity with a Carreau model. Using experimentally determined viscosity data for PEEK, effective properties of a fiber assembly were predicted. It was shown that the introduction of fibers into the fluid can dramatically decrease the maximum Newtonian strain rate. This is critical when determining a maximum strain rate for which Newtonian behavior is expected. The effect of the Carreau model parameters on the elongational viscosity were demonstrated for a wide range of values.

In addition to long discontinuous fiber systems, the relationships presented in this paper, all but the longitudinal elongational viscosity prediction, are valid for continuous fiber systems. It should be kept in mind that these relations provide insight into the relative magnitudes of the predicted properties, the effect of material descriptors, and the degree of anisotropy of the medium.

The influence of fiber orientation upon the effective viscosities of a medium consisting of discontinuous fibers suspended in a viscous medium have been determined for the conditions of perfect collimation and off-axis orientation, as well as ensemble misorientation. In the former case extreme sensitivity to fiber orientation was exhibited by all the viscosity terms corresponding to materials with aspect ratios of 10^3 - 10^4. Reduction in the ratio of apparent elongational viscosity to principal elongational viscosity of 10^{-3} for an orientation of 1° was observed.

The compliance matrix was utilized to predict the expected values for the anisotropic viscosities of the medium consisting of an ensemble of misoriented fibers in a viscous medium. This averaging approach yielded results for the expected values of viscosities which display the same tendencies as the properties for the off axis perfect collimation results. It was shown that small misalignments in

the fibers could greatly decrease the longitudinal elongational viscosities without corresponding effects on the transverse elongational and inplane shearing viscosities.

REFERENCES

1. R. B. Pipes, J. W. S. Hearle, R. K. Okine, A. J. Beaussart, and A. M. Sastry, "A Constitutive Relation for the Viscous Flow of an Oriented Fiber Assembly," submitted for publication, J. Comp.Mat., 1991.

2. R. B. Pipes, J. W. S. Hearle, A. J. Beaussart, and R. K. Okine, "Influence of Fiber Length on the Viscous Flow of an Oriented Fiber Assembly," submitted for publication, J. Comp. Mat., 1991.

3. R. B. Pipes, "Anisotropic Viscosities of an Oriented Fiber Assembly with a Power Law Matrix Fluid," submitted for publication, J. Comp. Mat., 1991.

4. D. W. Coffin, R. B. Pipes, "Anisotropic Viscosities of an Oriented Fiber Assembly," Proceedings of ICC8, Honolulu, Hawaii, July 15-19, 1991.

5. P. J. Carreau, "Rheological Equations from Molecular Network Theories," Trans. Soc. Rheol., 16 (1), pp. 99-127 (1972).

6. P. J. Carreau, D. DeKee, and M. Daroux, "An Analysis of the Viscous Behavior of Polymeric Solutions," Can. J. Chem. Eng., 57, pp. 135-140 (1979).

7. Z. Kemblowski and M. Michniewicz, "Correlation of Data Concerning Resistance to Flow of Generalized Newtonian Fluids Through Granular Beds," Rheol. Acta, 20, pp. 352-359 (1981).

8. L. E. Taske, Personal Communication, BASF, Charlotte, NC, (1990).

9. J. F. Pratte, W. H. Krueger, and I Y. Chang, "High Performance Thermoplastic Composites with Poly(ether keytone keytone) Matrix," Proceedings of the 34th International SAMPE Symposium, Reno, May 8-11, 1989, pp. 2229-2242.

Table 1

Anisotropic Viscosity Predictions [3]

Term	Newtonian Fluid
η_{11}/η	$\frac{f}{2}\left[\frac{1-\mu}{\mu}\right](L/D)^2$
η_{12}/η	$\frac{1}{2}\left[\frac{1+\mu}{\mu}\right]$
η_{23}/η	$\frac{1}{\mu}$
η_{22}/η	$\frac{4}{\mu}$

$$\mu=1-\sqrt{\frac{f}{F}}$$

Table 2

Plane Stress Orthotropic Viscosities

Volume fraction : 0.6 Packing geometry : square array	Micromechanics Predictions [3] $\eta_{11}/\eta = 2.08\ (L/D)^2$ $\eta_{12}/\eta = 4.47$ $\eta_{22}/\eta = 31.8$

Nomenclature

Symbol	Term	Units [F,L,T,D]
A_T	Temperature shift factor	--
D	Fiber diameter	L
f	Fiber volume fraction	--
F	Maximum fiber volume fraction	--
L	Fiber length	L
n	Power law exponent	--
T	Temperature	D
T_0	Reference temperature	D
$\dot{\varepsilon}_N$	Maximum Newtonian strain rate	1/T
η	Fluid viscosity	FT/L^2
η_0	Zero-shear viscosity	FT/L^2
η_{11}	Longitudinal elongational viscosity	FT/L^2
η_{22}	Transverse elongational viscosity	FT/L^2
η_{12}	In-plane shearing viscosity	FT/L^2
η_{23}	Transverse shearing viscosity	FT/L^2
λ	Time constant	T
ξ	Temperature shift factor constant	--
m	cos θ	--
n	sin θ	--
β_{ij}	Terms of the compliance matrix	$(Pa\text{-}Sec)^{-1}$
θ	Orientation angle	degree
η	Matrix viscosity	Pa-Sec
η'_{11}	Apparent elongational viscosity	Pa-Sec
η'_{22}	Apparent transverse elongational viscosity	Pa-Sec
η'_{12}	Apparent inplane shearing viscosity	Pa-Sec
$\langle\eta_{ij}\rangle$	Expected value of η_{ij}	Pa-Sec
ϕ	Probability density function	--

Figure Captions

Figure	Caption
1	Experimental Data for Viscosity Versus Shear Rate for PEEK at 399°C
2	Experimental Data for Temperature Shift Factor Versus Temperature for PEEK
3	Effective Viscosities Versus Strain Rate for Fiber Reinforced PEEK at 399°C
4	Effect of Temperature on Inplane Shearing Viscosity Versus Strain Rate for Fiber-Reinforced PEEK
5	Effect of Power Law Exponent on Longitudinal Elongational Viscosity Versus Strain Rate
6	Effect of Time Constant on Longitudinal Elongational Viscosity Versus Strain Rate
7	Effect of Temperature on Longitudinal Elongational Viscosity Versus Strain Rate
8	Influence of Fiber Orientation on Longitudinal Elongational Viscosity
9	Influence of Fiber Orientation on Transverse Elongational Viscosity
10	Influence of Fiber Orientation on Inplane Shearing Viscosity
11	Expected Value for Longitudinal Elongational Viscosity
12	Expected Value for Transverse Elongational Viscosity
13	Expected Value for Inplane Shearing Viscosity

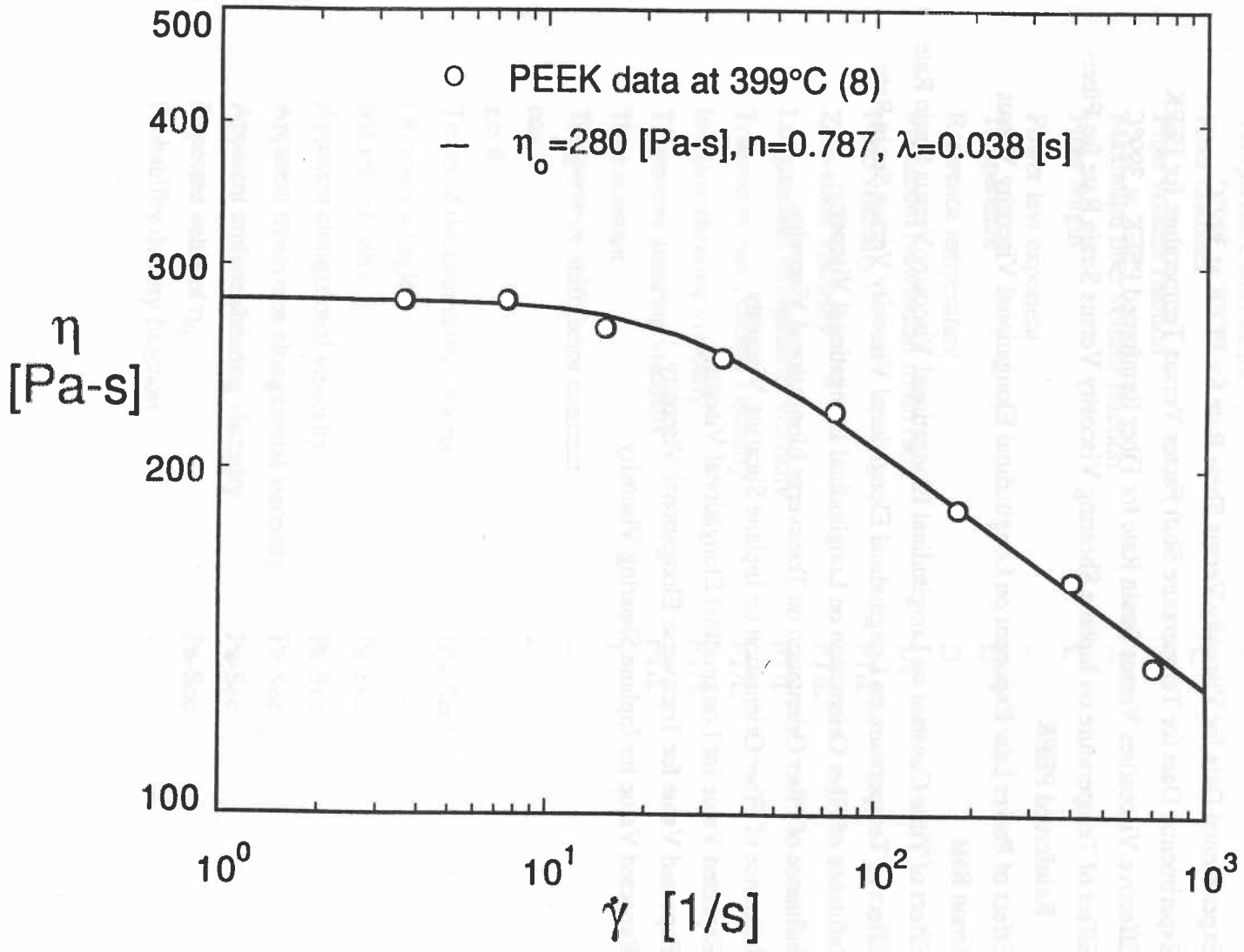

Fig. 1 Experimental Data for Viscosity Versus Shear Rate for PEEK at 399°C

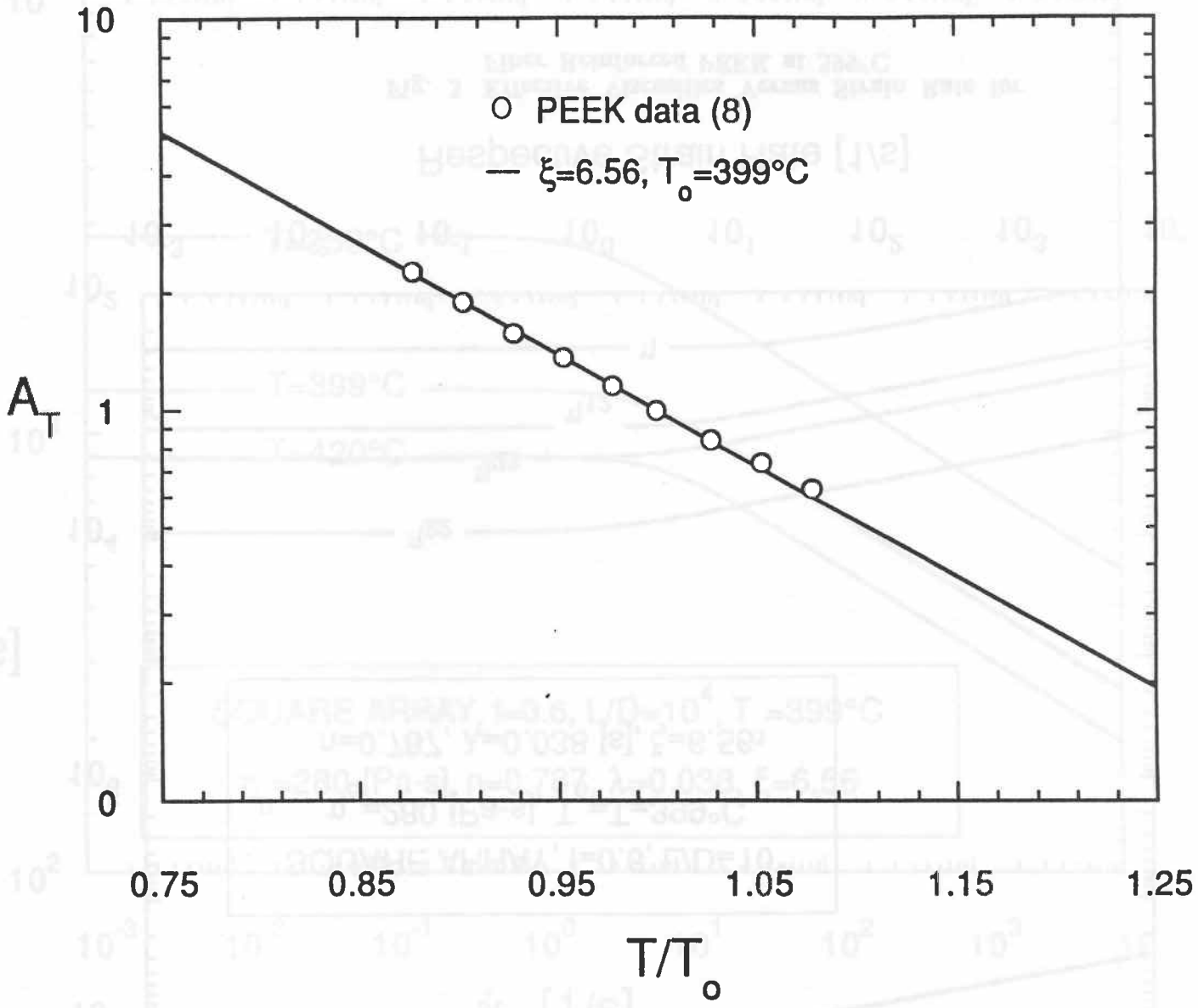

Fig. 2 Experimental Data for Temperature Shift Factor Versus Temperature for PEEK

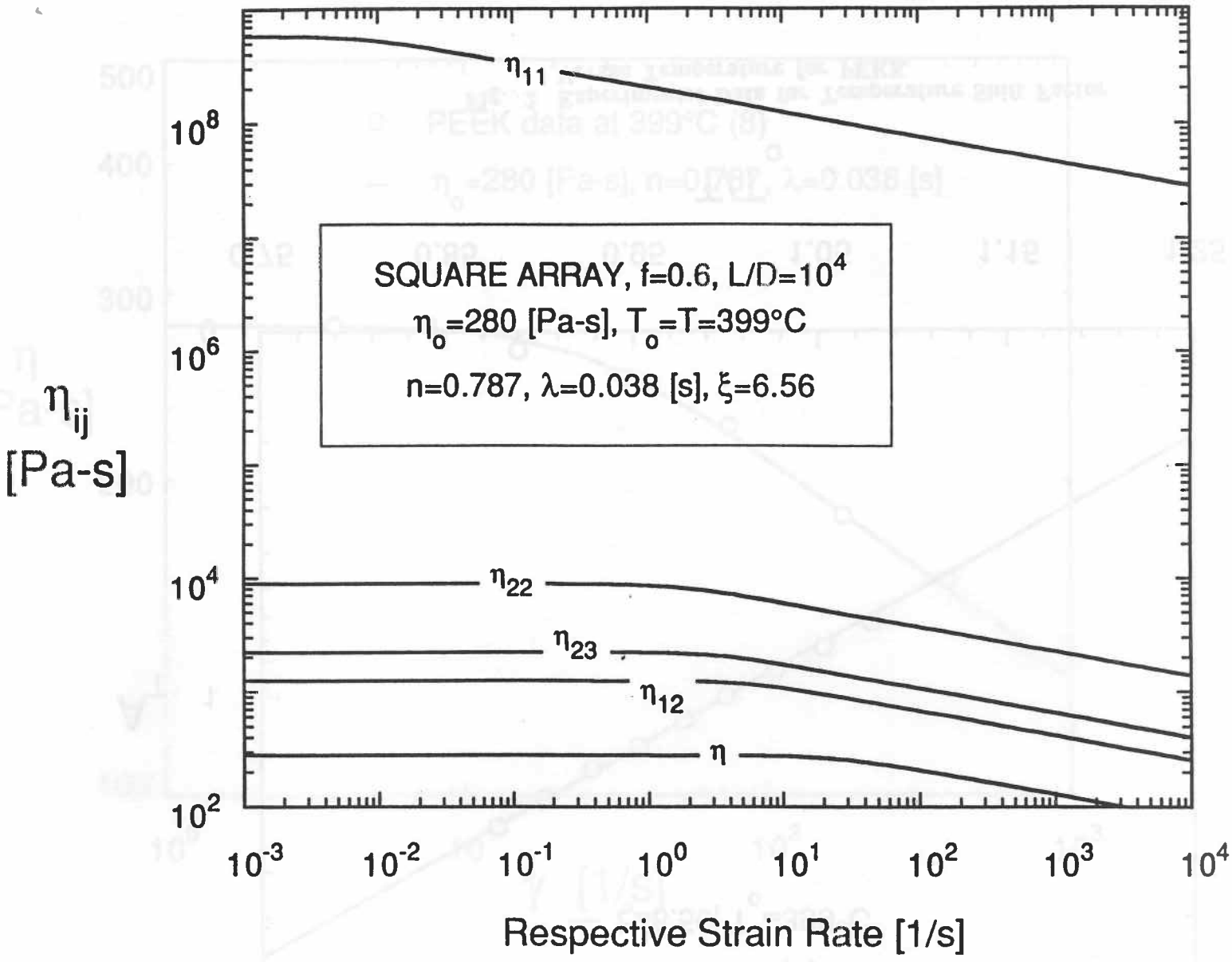

Fig. 3 Effective Viscosities Versus Strain Rate for Fiber Reinforced PEEK at 399°C

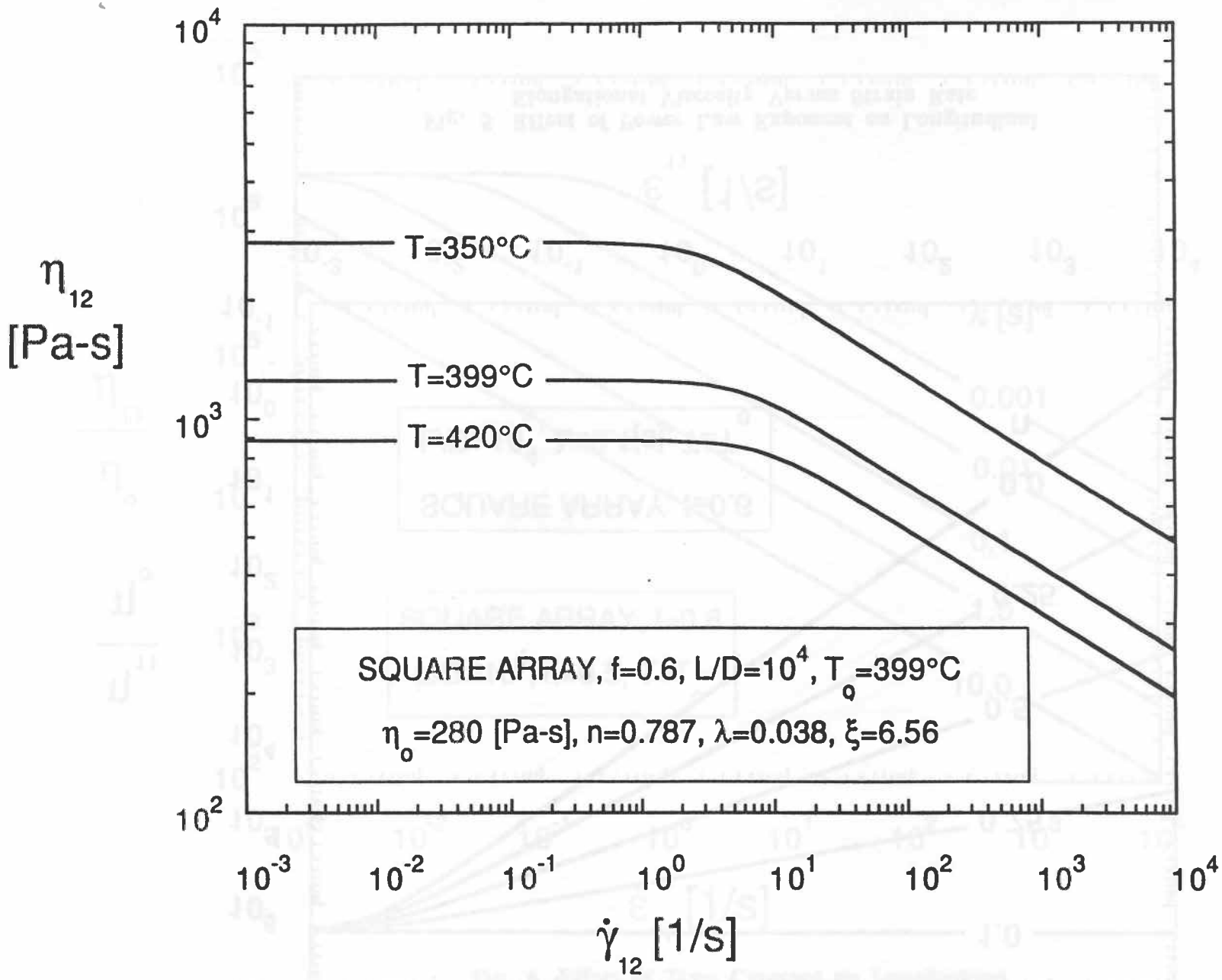

Fig. 4 Effect of Temperature on Inplane Shearing Viscosity Versus Strain Rate for Fiber-Reinforced PEEK

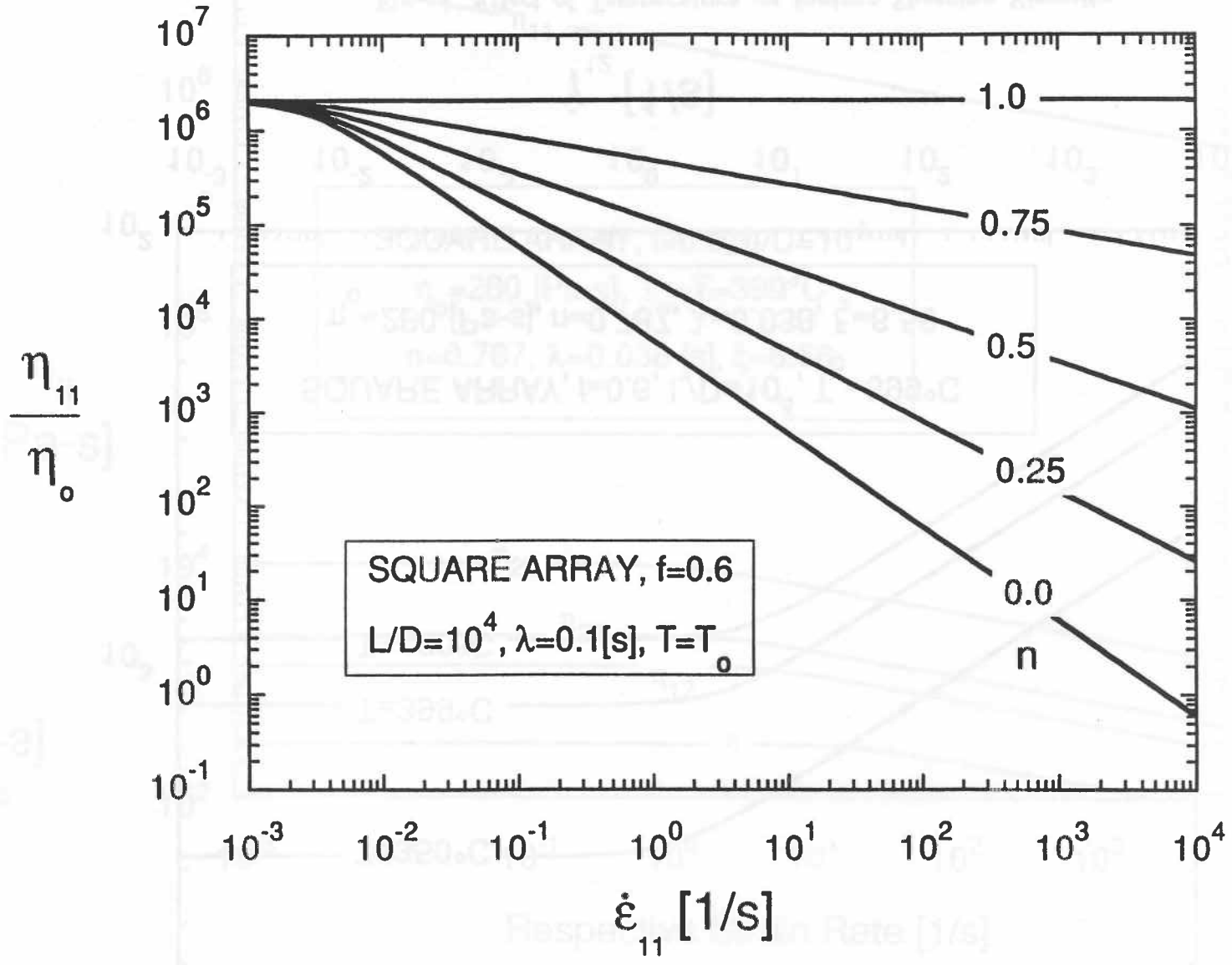

Fig. 5 Effect of Power Law Exponent on Longitudinal Elongational Viscosity Versus Strain Rate

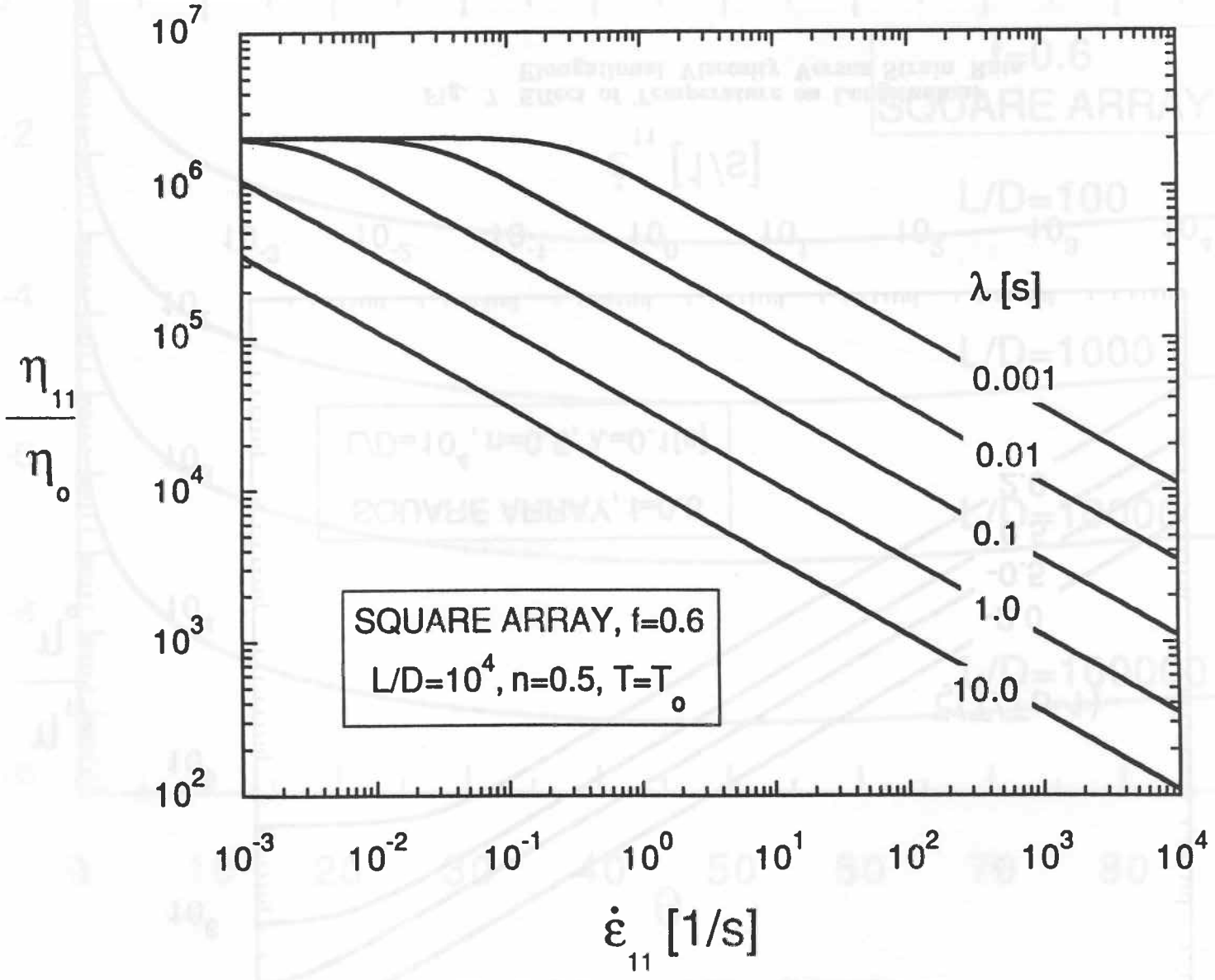

Fig. 6 Effect of Time Constant on Longitudinal Elongational Viscosity Versus Strain Rate

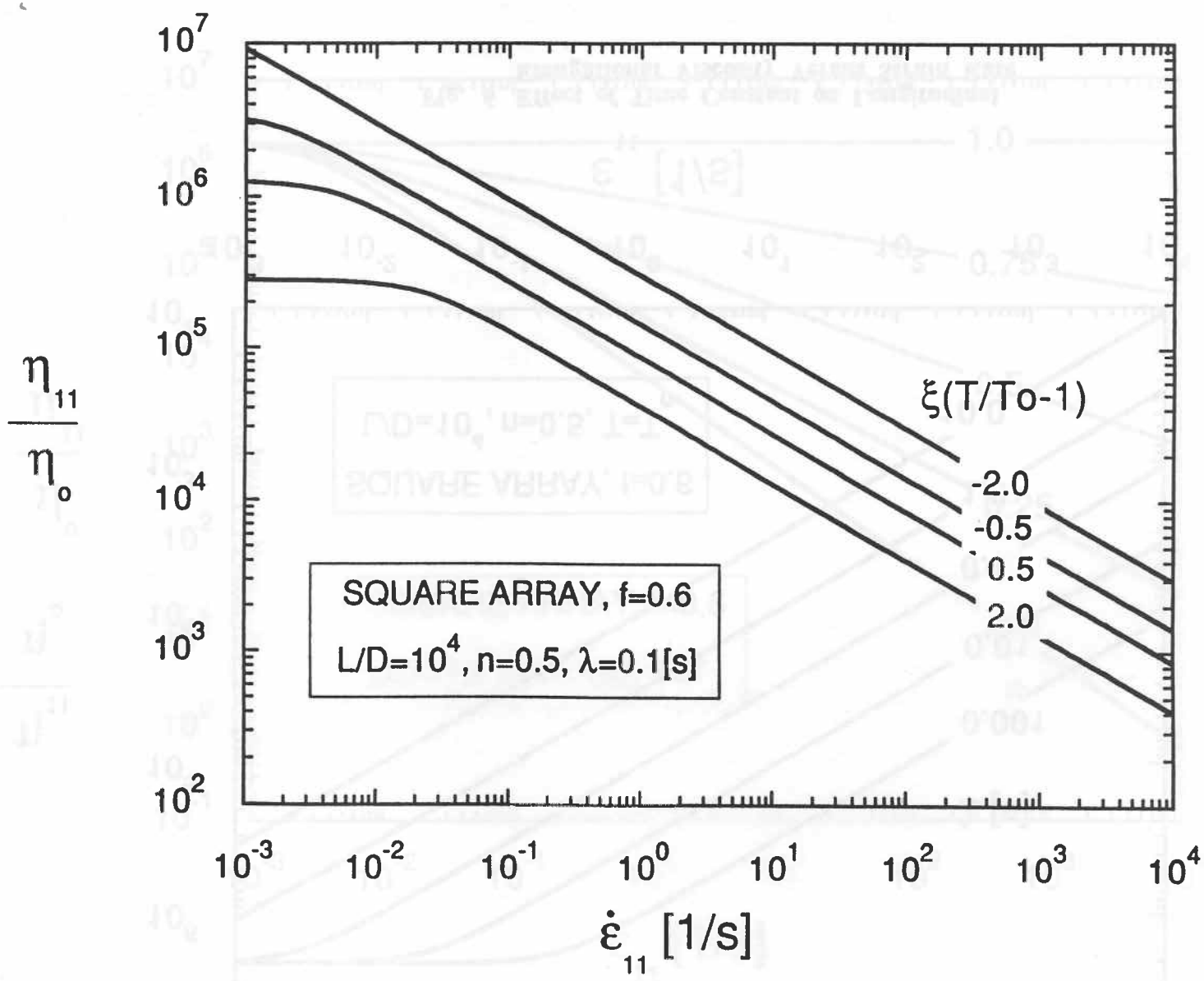

Fig. 7 Effect of Temperature on Longitudinal Elongational Viscosity Versus Strain Rate

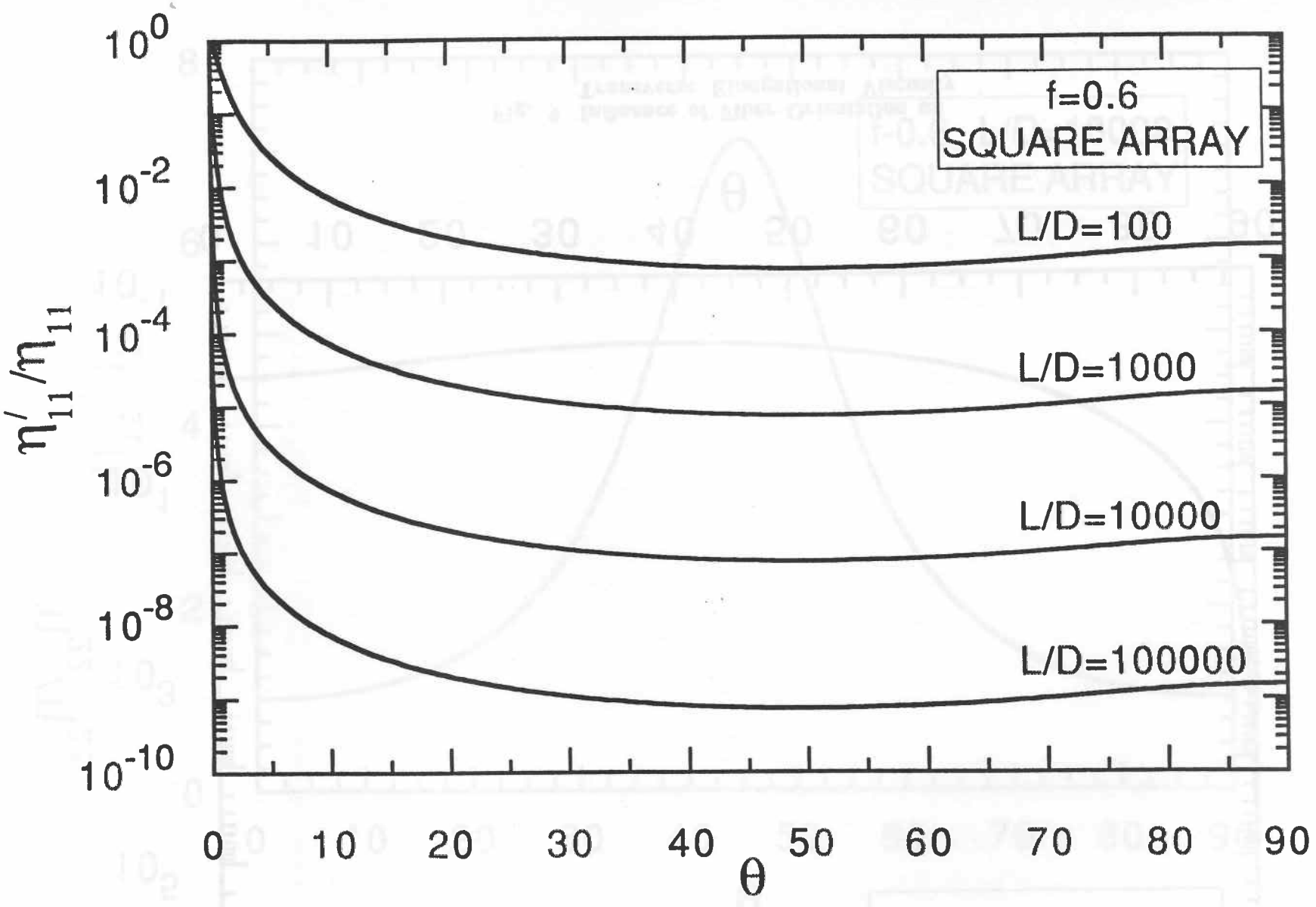

Fig. 8 Influence of Fiber Orientation on Longitudinal Elongational Viscosity

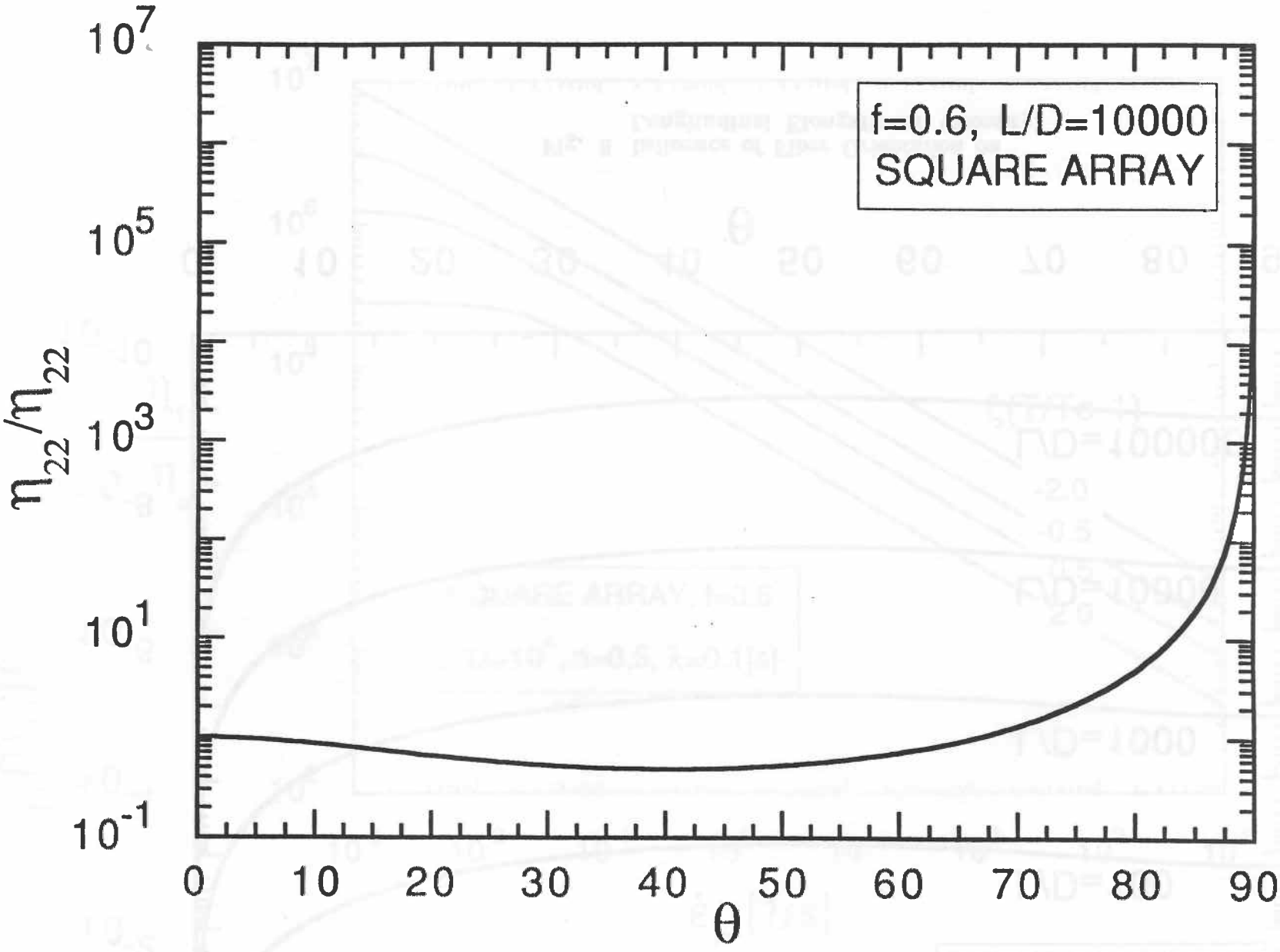

Fig. 9 Influence of Fiber Orientation on Transverse Elongational Viscosity

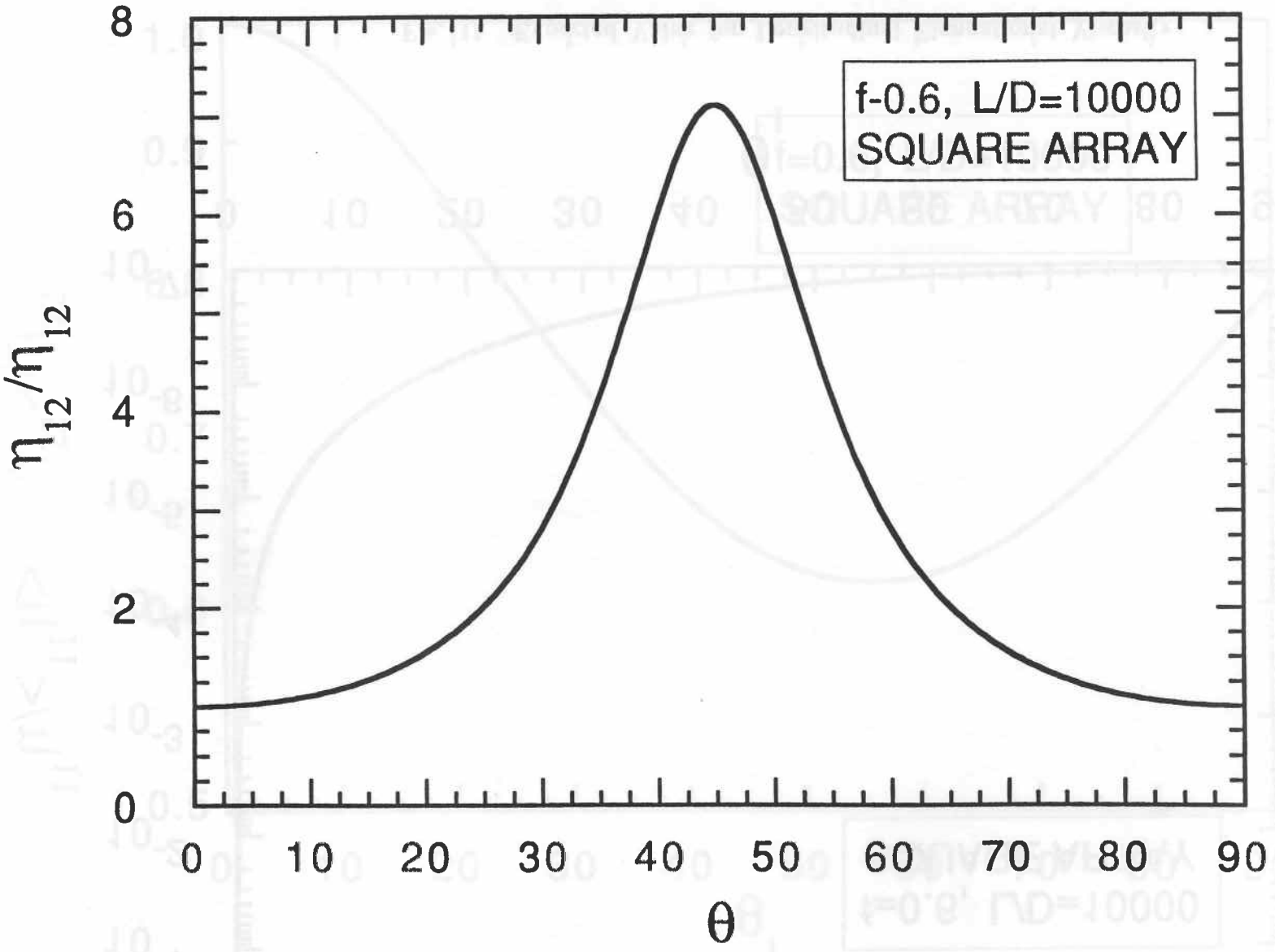

Fig. 10 Influence of Fiber Orientation on Inplane Shearing Viscosity

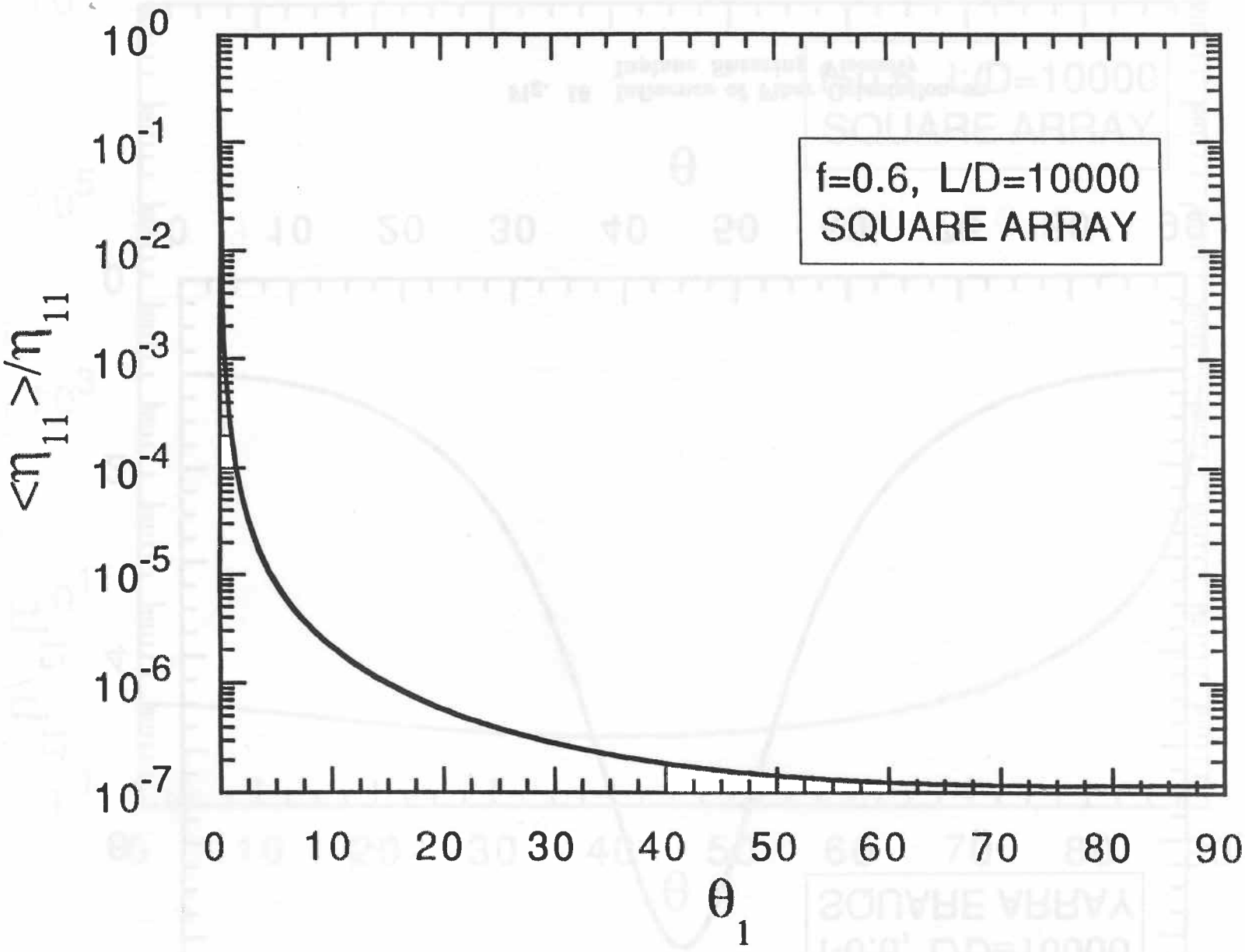

Fig. 11 Expected Value for Longitudinal Elongational Viscosity

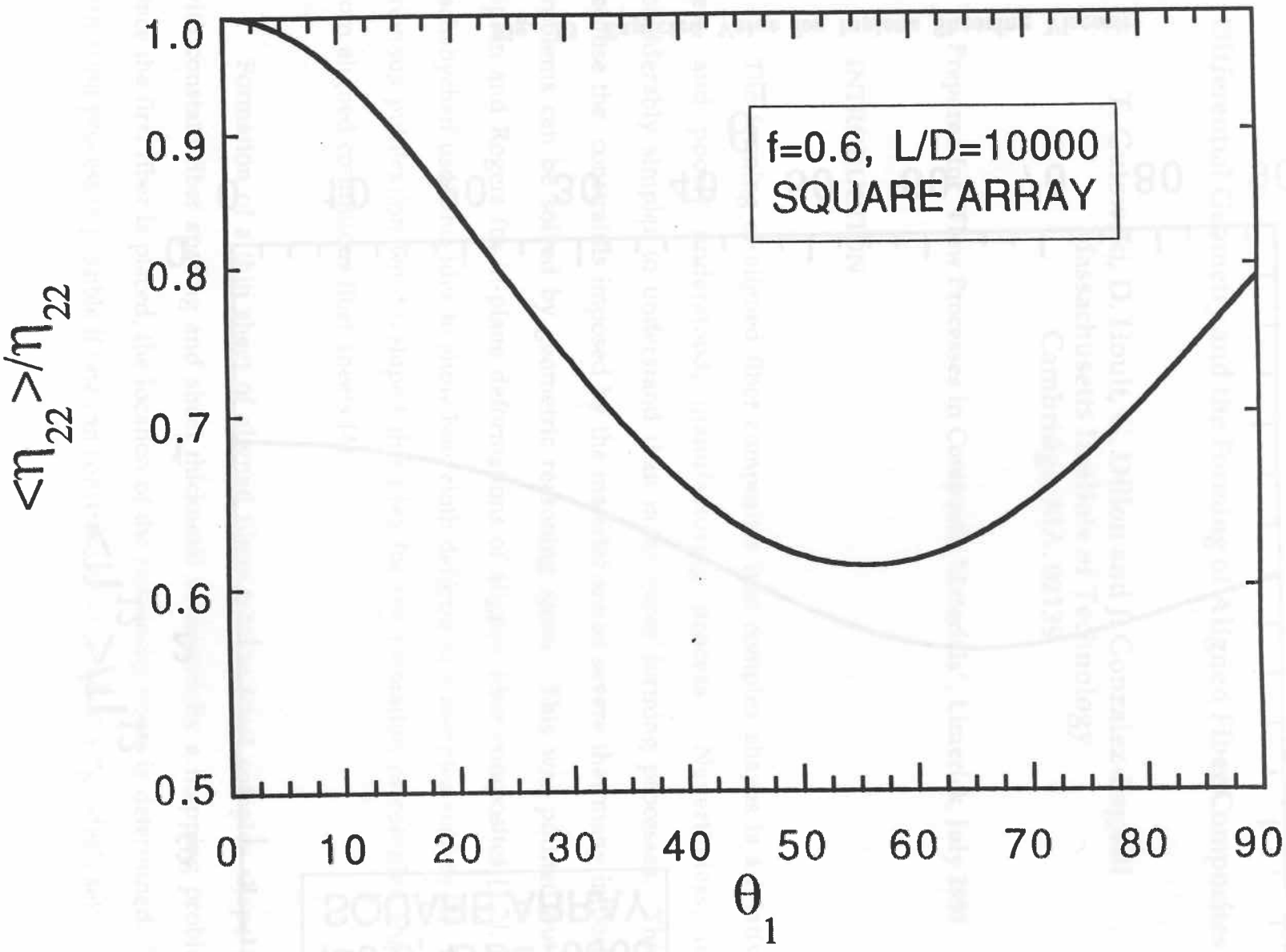

Fig. 12 Expected Value for Transverse Elongational Viscosity

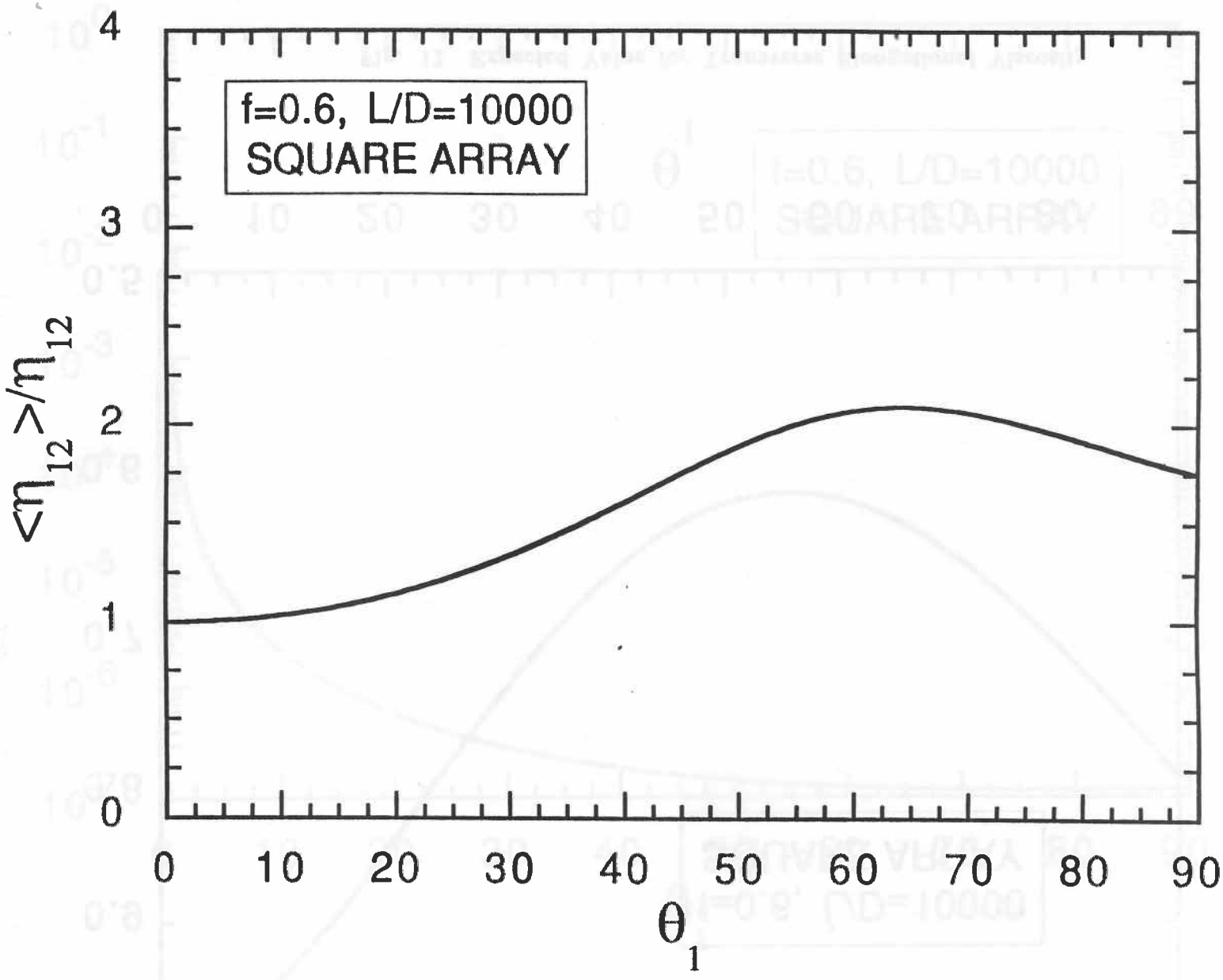

Fig. 13 Expected Value for Inplane Shearing Viscosity